Journal of Membrane Science 713 (2025) 123304

Contents lists available at ScienceDirect

Journal of Membrane Science

journal homepage: www.elsevier.com/locate/memsci

Highly selective thin B-oriented MFI zeolite membranes on scalable modified stainless steel supports

Fateme Banihashemi, Wen-Hsiung Lai, Jerry Y.S. Lin *

School for Engineering of Matter, Transport & Energy, Arizona State University, Tempe, AZ 85287, USA

ARTICLE INFO

Keywords:
B-oriented membrane
MFI zeolite
Xylene isomers separation
Thin film
Scalable substrate

ABSTRACT

Enhancing the separation performance of molecular sieve membranes relies significantly on precise control over their membrane morphology and microstructure. This involves creating thin, closely packed, oriented, and uniform coatings of seed crystals, enabling subsequent intergrowth to establish continuous membranes. To address industrial needs, it is crucial to generate a thin and flawless membrane efficiently producible on a large-scale support. Porous stainless supports offer scalability and easy integration into membrane modules. In this study, we present a novel and straightforward process for modifying stainless-steel supports to seed zeolite membrane layers. High-performance, b-oriented MFI zeolite membranes can be synthesized on these modified stainless-steel supports through scalable filtration seeding of MFI zeolite nanosheets followed by secondary growth. By employing a carefully designed pre-treatment procedure, we achieved the growth of well-intergrown, highly b-oriented MFI zeolite membranes on the modified stainless-steel support, establishing a robust interaction with the substrate. The membranes, fabricated through gel-free secondary growth of nanosheets deposited on a scalable stainless-steel support using this technique, demonstrate ultra-selective capabilities in separating para-xylene from ortho-xylene, with a high separation factor of 388.

1. Introduction

MFI Zeolite thin films have displayed great potential as separation membranes [1,2], selective sensors [3,4], optical materials [5], adsorbents [6,7], and catalytic coating reactors [8,9]. This has led to an increase in interest in making zeolite membranes for use in various fields. The molecular sieving properties of MFI zeolite membrane can be greatly impacted by the orientation of its constituent micro-crystals. Particularly, the b-oriented MFI membranes show exceptional separation performance as separation membranes due to having the straight channel along the b-axis which is the fastest diffusion pathway in MFI crystals [10]. MFI zeolite membranes, particularly b-oriented ones, have potential for industrial processes involving separation of xylene isomers and other hydrocarbon/H_2 mixtures [11,12].

Over the past few years, nanosheet crystals with nanometer-scale thickness have become highly desirable for separation applications. This is because their thin dimension allows shorter diffusion paths [10]. In essence, it is possible to apply uniform and thin coatings of high-aspect-ratio zeolite nanosheets onto almost any porous membrane substrate. Subsequently, a final step of secondary zeolite growth can be carried out to seal the nanoscopic gaps between the nanosheets, resulting in molecular sieving membranes with high flux [11].

To date, various techniques have been developed to create MFI nanosheets with different microstructures. Tsapatsis and coworkers synthesized high-aspect ratio MFI zeolite crystals through a top-down exfoliation process of 2D MFI layered stacks and later a bottom-up growth process using single rotational intergrowth-triggered crystals [12–14]. Hedlund and coworkers employed a different approach to synthesize hydrophobic MFI nanosheets through prolonged aging in the fluoride medium. However, these synthesis methods feature very complicated and lengthy synthesis procedure [15]. Recently, Liu and coworkers [16] developed a new and facile method for preparing thin MFI nanosheets using a progressive wall-thinning approach. The MFI nanosheets produced by this method have a high aspect ratio, are highly uniform, and are produced efficiently with high yields.

Efforts have been made to create high-quality b-oriented zeolite membranes reproducibly. New techniques for growing b-oriented MFI zeolite membranes were developed using solvent-assisted and gel-less secondary growth methods. According to the literature [10], the b-oriented MFI membranes prepared by gel-free secondary growth of these

* Corresponding author.
E-mail address: Jerry.Lin@asu.edu (J.Y.S. Lin).

https://doi.org/10.1016/j.memsci.2024.123304
Received 26 July 2024; Received in revised form 3 September 2024; Accepted 5 September 2024
Available online 6 September 2024

nanosheets show improved performance, compared to the membranes prepared by other secondary growth methods. These gel-free secondary grown b-oriented MFI zeolite membranes show separation factor of p-xylene over o-xylene of 2000–8000. These results signify separation power of b-oriented MFI membranes made from nanosheets for xylene isomer separations.

However, the current process of fabricating these MFI membranes presents significant challenges regarding practical feasibility and scalability [11]. In this process, defect free b-oriented membranes for xylene separation were fabricated on porous Stöber silica or modified silica fiber-derived disk-type supports [17,18]. These supports have low mechanical strength [11,18]. It is known that the growth of zeolite membranes is greatly influenced by the physical structure and chemical properties of the support. Therefore, selecting the right type of support is extremely important [19,20]. For industrial applications, the b-oriented MFI zeolite membranes should be deposited on supports which can be readily arranged into modules of high packing density. Thus, creating 2D MFI nanosheet-based membranes on easy-to-produce and cost-effective macroporous supports is critical to industrial applications of these membranes.

Taking into consideration some factors such as cost, thermal conductivity, anticorrosion quality, mechanical strength, scalability and fictile properties, porous stainless-steel material is a very promising support for a microporous membrane. However, due to significant differences in surface properties between stainless steel material and zeolites, it is challenging to grow zeolite membranes on the stainless-steel surface. To overcome this issue, the surface of the stainless-steel surface should be adequately modified for zeolite membrane growth [11,19]. The objective of this paper is to modify the surface of porous stainless-steel supports by different Si-derived intermediate layers for synthesizing high quality and thin b-oriented MFI zeolite membranes from MFI zeolite nanosheets for xylene isomer separation.

2. Experiment

2.1. Modification of stainless-steel support

Porous stainless-steel plates (316L) of 20 mm in diameter and 2 mm in thickness (Mott company, 0.2-A −316LSS) were used as supports (substrates) to grow the b-oriented MFI zeolite membranes. The bare substrates were cleaned by sonication in acetone for 30 min. To modify the stainless-steel substrates, Al–Si alloy (Al: 87–89 %, Si:11–13 %, 1–2 μm, Sky Spring Nanomaterials, Inc.), Si (80 nm, Sky Spring Nanomaterials, Inc.) and in-house synthesized 50 nm SiO_2 powders were used.

The Al–Si alloy particles were coated via a hot-drop coating (HDC) approach. Firstly, the 0.05 wt% suspension of alloy in water was prepared. Sodium hydroxide (NaOH, >97 %, Sigma Aldrich) was added to the suspension to adjust its pH to 9. To guarantee complete dispersion, the suspension was sonicated for approximately 10 min. A bare stainless-steel substrate was preheated to the temperature of 140 °C on a heating platform. Then, 1 ml colloidal suspension mentioned above was slowly dropwise coated on the substrate to ensure the thorough evaporation of water and compel a staggered stacking pattern of the particles. Finally, the obtained stainless-steel substrate coated with the alloy was dried completely at the coating temperature for 5 min and then heat-treated at 560 °C under Argon atmosphere. The 80 nm Si particles were gently rubbed on the surface of substrate coated with the alloy to obtain a uniform layer and then heat-treated at 900 °C for 2 h with the cooling and heating rate of 10 °C/min.

The 50 nm SiO_2 particles were synthesized in our lab according to the StÖber procedure [21] using two solutions with the compositions given in literature [22]. 4.5 ml tetraethyl orthosilicate (TEOS, 98 %, Sigma Aldrich) and 35.6 ml 200 proof ethanol were mixed separately in room temperature. This solution was added into the solution of 0.6 ml ammonium hydroxide (NH_4OH, 28.0–30.0 % NH_3 basis, Sigma Aldrich), and 19.3 mL distilled water. The resultant solution was stirred for 2h at room temperature. White colloidal particles formed in the solution were collected by centrifugation (10,000 rpm) and washed 3 times in ethanol. Particles were dried at 50 °C overnight and calcined at 400 °C for 3 h with heating and cooling rates of 2 °C/min and 4 °C/min, respectively. The resulting powder was crushed in an agate mortar and was used for modifying the surface of the supports. The SiO_2 particles were then coated on the Al–Si alloy and Si coated substrate by the rubbing method and were calcined in the furnace at 500 °C for 5h.

2.2. Synthesis of MFI zeolite nanosheets and membranes

To synthesize parent MFI crystals, a synthesis solution was prepared by adding tetraethyl orthosilicate (TEOS, 98 %, Sigma Aldrich) as a silica source to a solution of tetra propylammonium hydroxide (TPAOH, 1 M, Sigma Aldrich) and water under stirring at room temperature for 24 h till a clear synthesis solution was obtained. The solution, with a molar composition of 1 TEOS: 0.15 TPAOH: 103.5 H_2O, was then allowed to age at room temperature for 48h, then filtered through a filter paper (Whatman No. 5) and directly loaded into a Teflon-lined stainless-steel autoclave. The hydrothermal synthesis was carried out at 170 °C for 10 h under rotation in a rotary reactor. The autoclave was then cooled naturally to room temperature, then the silicate crystals were collected through centrifugation and washed carefully with deionized water. The synthesized MFI crystal powder was finally dried at 70 °C for 12 h and calcined at 550 °C for 6h.

For 3.5 μm sized MFI nanosheet, 0.2 g of calcined 5.5 μm–sized parent MFI crystals was added in 15 g of 0.235 M TPAOH solution. Prepared suspension was then transferred into a Teflon-lined stainless-steel autoclave. Hydrothermal treatment was carried out at 170 °C for 24 h in a rotational convection oven (70 r/min). Obtained solid precipitates were washed with deionized water and collected by centrifugation. This rinsing process with deionized water was repeated three times. The recovered MFI nanosheet slurry (about 0.2 g)was then dispersed in 60 ml deionized water for filtration coating.1 ml of freshly prepared MFI nanosheet dispersion (made from 60 ml, as described above) was mixed with 10 ml of deionized water and sonicated for around 10 min. The resulting suspension was then coated onto modified stainless steel supports using vacuum-assisted filtration. To slow the filtration process, the vacuum was maintained at around 1.5 psi during coating. The coating process typically took around 1 h and was followed by 1 h of vacuum drying to ensure complete drying. The coating process was repeated 1 to 2 times as needed until the surface of substrates was completely covered by MFI nanosheets.

The b-oriented MFI zeolite membranes were prepared by gel-less-steam-assisted crystallization method. To prepare the synthesis solution, tetra propylammonium bromide (TPABr, Sigma-Aldrich, 98 %) and sodium hydroxide (NaOH, Sigma-Aldrich, 97 %) were dissolved in distilled water, and then tetraethyl orthosilicate (TEOS, Sigma-Aldrich, 99 %) was slowly added under stirring. A clear solution with a molar composition of 0.45 TEOS: 0.3 TPABr: 0.275 NaOH:139 H_2O was obtained after stirring at room temperature for 2–3 h. The modified supports coated with the zeolite nanosheets were dipped into the clear solution for 20 s and dried at 100 °C for 15 min. The process of dip coating–drying was repeated 2–3 times and then the coated supports were transferred to a Teflon-lined autoclave and placed on a sample holder horizontally. Before sealing, 1 g of deionized water was added to the autoclave. After heating at 180 °C for 24 h, the zeolite membrane was removed from the autoclave, washed with water and dried at 60 °C. The synthesized b-oriented MFI zeolite membranes were calcined at 400 °C for 12 h to remove the organic template.

2.3. Membrane characterization and xylene separation tests

The samples prepared in this work were characterized by PANalytical X-pert Pro MRD High Resolution X-ray Diffractometer (XRD),

with Cu Kα radiation ($\lambda = 1.542$ Å) at 40 kV and 40 mA and scan step of 0.05°, for phase structure and crystallinity. The surface and cross-sectional morphology of the samples was examined by scanning electron microscope (SEM) (Amray 1910), with sample preparation by Auriga (Zeiss) and SEM/FIB Focused Ion Beam - Helios 5 UX (Thermo Scientific). Fourier transform infrared (FTIR) (Thermo Nicolet 6700) was used for identifying surface functional groups of stainless-steel supports before and after modification with different layers.

Vapor permeation experiments were performed using a Wicke-Kallenbach [23] separation set-up, which was illustrated schematically in our previous publications [24,25]. Helium was used as the carrier gas for the feed, and as sweep gas. The feed and permeate were both maintained at 1 atm. The temperature of the module was kept within a range of 75–275 °C. The flow rate of helium in the feed and sweep was respectively controlled at 20 ml (STP)/min using mass flow controllers. Before entering the membrane module, the helium carrier gas was passed through a sparger containing a binary xylene mixture to saturate it with vapor, at p-xylene and o-xylene partial pressures respectively of ~0.49 kPa and ~0.55 kPa. To prevent xylenes from condensing, the membrane module and pipeline leading to the gas chromatograph (GC) were heated above the boiling point of xylene using an oven and heating tapes. The retentate and permeate streams were analyzed using a GC [Agilent Technologies GC-6890 N with a flame ionization detector (FID) and an HP-5 capillary column] to determine their compositions. The accuracy of pervaporation and vapor permeation results was ±5.0 % for the separation data of binary mixtures.

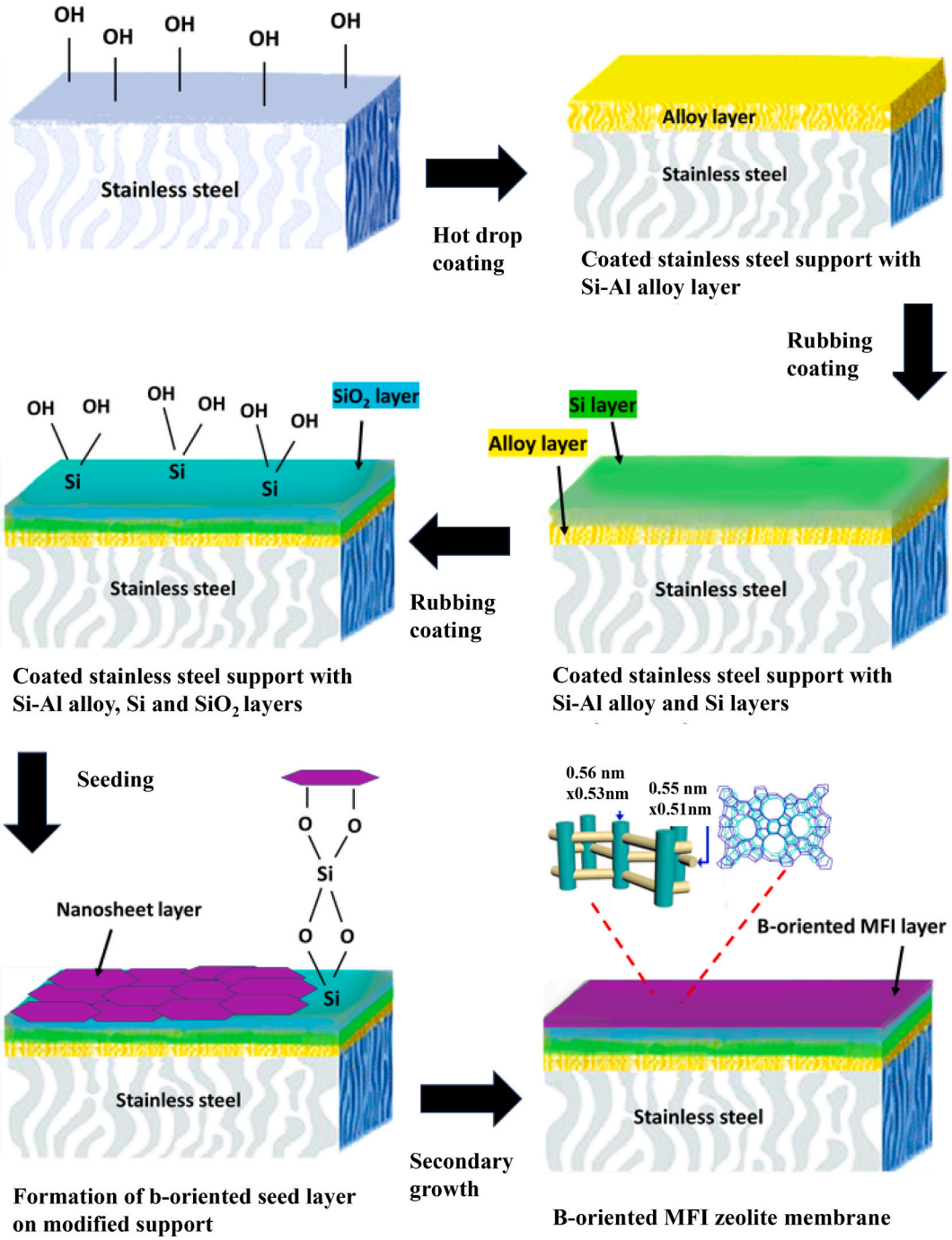

Fig. 1. Schematic illustration of steps/mechanism for modifying stainless support and formation of the b-oriented membrane on the modified stainless-steel substrate.

3. Results and discussion

Fig. 1 illustrates various steps in modification of and growing zeolite membrane on stainless support and mechanisms associated with these steps. The first few steps deal with modification of the porous stainless-steel disks. Experiments conducted in our lab showed that good quality MFI zeolite nanosheet seed layer could not be formed on stainless steel supports without a smooth silica layer using SiO_2 nanoparticles. Thus, a multiple-step surface modification strategy was adopted in order to coat the smooth SiO_2 layer on the support for growing high-quality b-oriented MFI zeolite membranes. This was done by hot-drop coating a suspension of Al–Si alloy beads, which were 1–2 μm in size, to reduce the surface roughness of the stainless-steel support. The supports were then coated with another thin layer of 80 nm Si particles by the rubbing method to further reduce its surface roughness. Finally, the stainless-steel support was coated with a thin layer of 50 nm silica particles by rubbing, which also enhanced the smoothness of support surface further, before the coating of MFI zeolite nanosheet seeds and secondary growth. The surface color of the stainless steel disks was silvery-gray or metallic, typical of stainless steel. After coating with Al–Si alloy, the color shifted to dark cyan and became slightly darker following heat treatment. When coated with Si powder, the surface color changed to brown, and it turned shiny brown after coating with SiO_2 powder. Following nanosheet coating, the surface became white, and it remained white after membrane growth. The results for each step will be presented and discussed next.

3.1. Characteristics of modification layer on stainless-steel substrates

Fig. 2(a)–(c) reveal that the Si–Al alloy, Si, and SiO_2 particles are of spherical shape with uniform size. Fig. 2(d) shows XRD patterns of the Al–Si alloys particles. As expected, only Al and Si reflections are visible. The crystal structure of Al–Si alloys can vary depending on the composition and processing conditions. The crystal structure of pure aluminium is a face-centered cubic (FCC) structure. The silicon atoms are often dissolved in the aluminium lattice. The primary silicon phase usually adopts a needle-like or plate-like morphology, and it has a diamond cubic crystal structure [26]. The broad peaks at the XRD pattern (Fig. 2(e) as pointed at $2\theta = 28.5°$, $47.4°$, $56.2°$, $69.3°$and $76.5°$correspond to the characteristic crystal peaks of Si which support a good crystalline structure with small crystallite size [27,28].

Fig. 3 shows scanning electron microscopy (SEM) top view images of the bare stainless-steel support, and the subsequent modified intermediate layers. The original stainless-steel substrates have quite a rough surface (with the porosity of 45 % and average pore diameter of 9 μm, respectively) (Fig. 3(a)). SEM micrographs show a smooth and uniform surface of substrate was achieved after modification sequentially with Al–Si alloy (Fig. 3(b)), Si particles (Fig. 3(c)) and silica powders (Fig. 3 (d)) synthesized in this work.

The FIB-SEM cross-sectional micrograph of modified stainless-steel substrate (Fig. 3(e)) displays distinct modification layers of porous morphology. The stainless-steel support and different coated layers can be easily identified. Fig. 3(f) displays the XRD patterns for the bare stainless-steel support, and the support coated with Si–Al alloy, Si, and SiO_2 layers. The modified substrates with various layers were analyzed using XRD after undergoing heat treatment. For the 316L stainless steel, typical austenite (1 1 1), (2 0 0) and (2 2 0) peaks can be observed. With the more modified layers coated on the surface of 316L stainless steel support, the peak intensity of stainless steel was decreased. XRD pattern belongs to Al–Si alloy which includes diffraction peaks from α-Al and Si respectively as documented in literature [29,30]. The alloy-coated substrates show all the diffraction peaks of both stainless-steel substrate and Al–Si alloy, confirming the formation of an alloy layer on the supports.

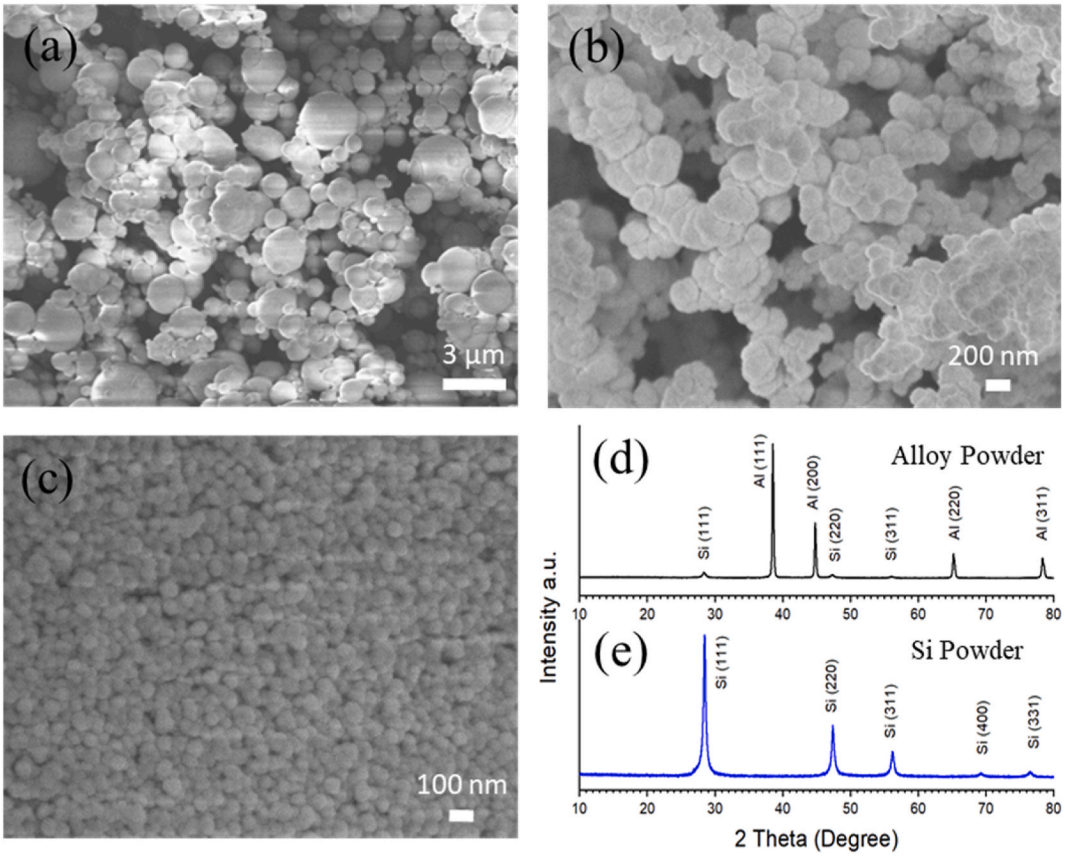

Fig. 2. SEM micrographs of powders of (a) Al–Si alloy, (b) Si and (c) SiO_2; XRD patterns of (d) Al–Si alloy and (e) Si particles (SiO_2 used is amorphous).

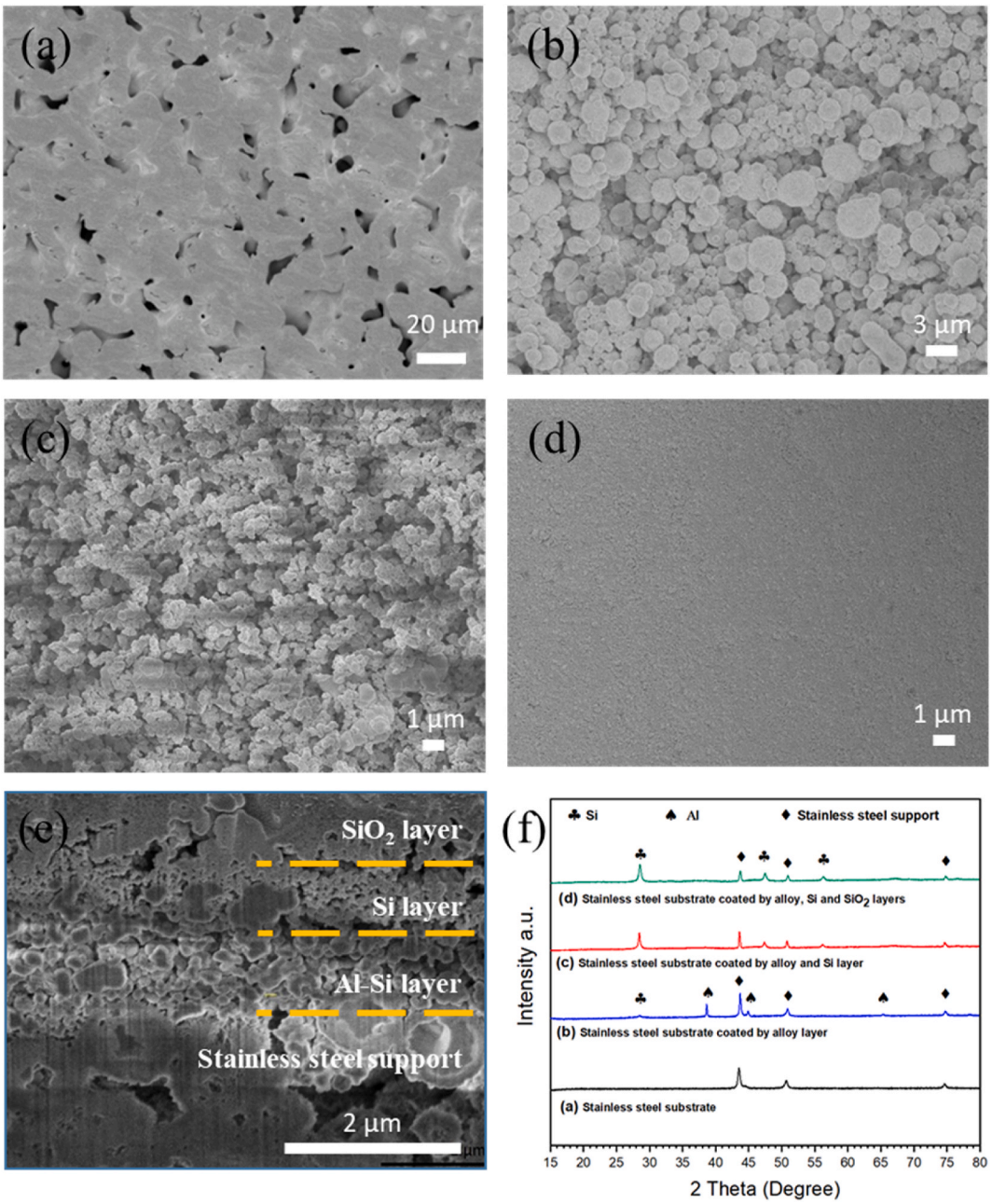

Fig. 3. SEM top-view of (a) the bare support; after coating with (b) Si–Al alloy powder; (c) 80 nm Si particles; and (d) 50 nm StÖber silica particles, (e) the FIB/SEM of substrate cross section of modified support and (f) XRD patterns of substrate without and with modification layers.

Fig. 4 shows the IR spectra of the stainless-steel substrate without and with Al–Si alloy, Si and SiO_2 modification layers. The IR spectra of Al–Si alloy coated support in the range of 1034–1075 cm^{-1} bands due to the asymmetric stretching vibrations of Si O(Si) and Si O(Al) connections are observed [31,32]. The peak in the range of 616–625 cm^{-1}, originates from the Si–Si bonds vibrations for the sample coated Si [33]. The spectrums of Si and SiO_2 coated support show broad band around 1625 cm^{-1} which represents the bending vibration of OH. The spread band between 1300 and 1000 cm^{-1} and peaked at 1080 cm^{-1} attribute to asymmetric stretching vibration to siloxane bonding of Si–*O*–Si bridges. The IR band at 951.21 cm^{-1} is symmetric stretching vibration of silanol Si–OH on the surface. The absorption band at 801.21 cm^{-1} corresponds to the symmetric stretching vibration of Si–*O*–Si bonding. The IR peak at 460 cm^{-1} is associated with an asymmetric deformation vibration bonding of O–Si–O [34]. The chemical groups present on both the unmodified and altered stainless-steel support are indicated in Figs. 1 and 4.

In order to determine the appropriate heat treatment temperatures for the Si–Al alloy layer, XRD patterns of samples heat-treated at varying temperatures were measured and are shown in Fig. 5. The results show no new phases emerged because of the modification process. The resulting alloy layer exhibits outstanding adhesion to the metal substrate when exposed to temperatures exceeding 560 °C compared to lower temperatures in which the peeling off issue was observed. However, the peak intensity of Al decreases with the increasing temperature of heat treatment process.

The intensity of the XRD peaks associated with the Si–Al alloy decreases drastically as the heat treatment temperature rises, which is attributable to the alloy elements diffusing into the substrate at high temperatures [35,36]. When depositing an alloy suspension onto a porous surface, the particles in the initial drops tend to settle into the larger pores. As deposition continues, subsequent drops lead to a

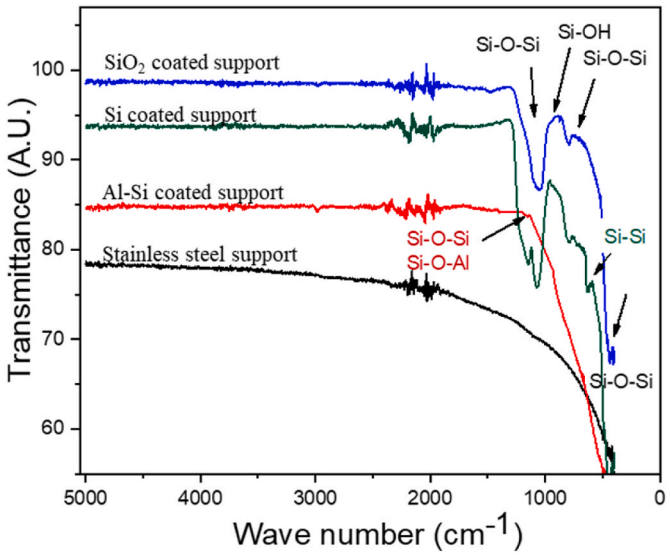

Fig. 4. FT-IR spectra of substrate with different modification layers.

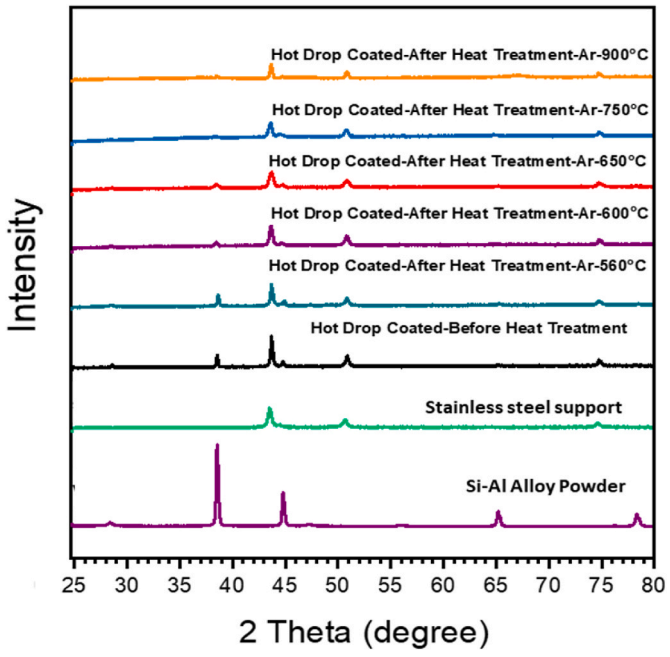

Fig. 5. XRD pattern of stainless-steel substrates coated with Si–Al alloy heat treated at different temperatures.

complete and uniform coverage of the substrate surface. This results in the formation of areas that penetrate the surface in a direction perpendicular to the substrate interface at high temperatures. As a result, the thickness of the alloy layer is reduced due to the presence of pores and valleys on the porous substrate surface. This process is illustrated schematically in Fig. 6.

Moreover, the diffraction peak intensities of Al phase for the Si and SiO_2 coated substrates (Fig. 2(d)) are much weaker than that in the alloys coated sample, and even the Al (111), (200), (220) and (311) peaks vanish in the patterns c and d. XRD patterns of Si-coated support before and after heat treatment shown in Fig. 7 confirm this phenomenon. The dashed arrows indicate disappeared Al peaks after heat treatment at 900 °C. This is related to the intermetallic diffusion of the alloy layer in stainless-steel substrate at high temperatures, as observed in Fig. 6.

3.2. Structure and separation performance of B-oriented MFI zeolite membranes

The parent MFI zeolite crystals were synthesized through a straightforward hydrothermal method and have a consistent coffin-shaped morphology measuring 5.5 μm × 2.5 μm × 0.95 μm (Fig. 8 (a)). These crystals have an aspect ratio (lateral length to thickness ratio) of about 6. The MFI zeolite nanosheets derived from the parent MFI zeolite by the modified process reported in literature [16] are thinner, approximately 45 nm in thickness, leading to a significantly increase in aspect ratio to about 100. The straight pore channels of 0.56 nm × 0.54 nm are vertical to the nanosheet in the [0*k*0] crystallographic direction. SEM micrograph confirms that a continuous, and dense coating of highly b-oriented 2D MFI nanosheets is obtained on the surface of modified

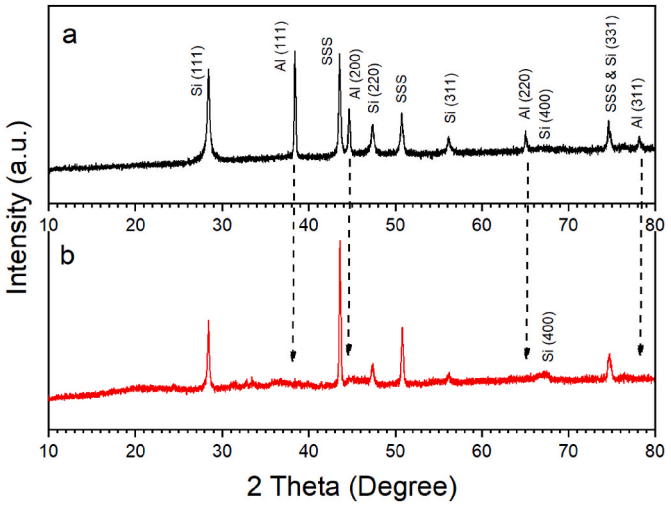

Fig. 7. XRD pattern of stainless-steel substrates coated with Si–Al alloy and Si layer (a) before and (b) after heat treatment at 900 °C.

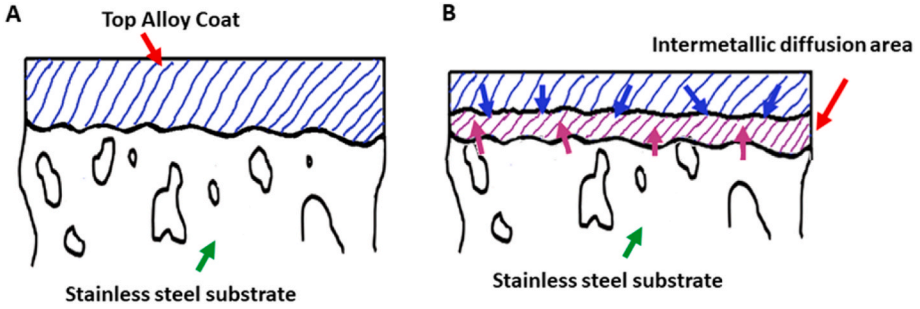

Fig. 6. Schematic diagram Si–Al alloy coat on stainless-steel support (a) before and (b) after heat treatment.

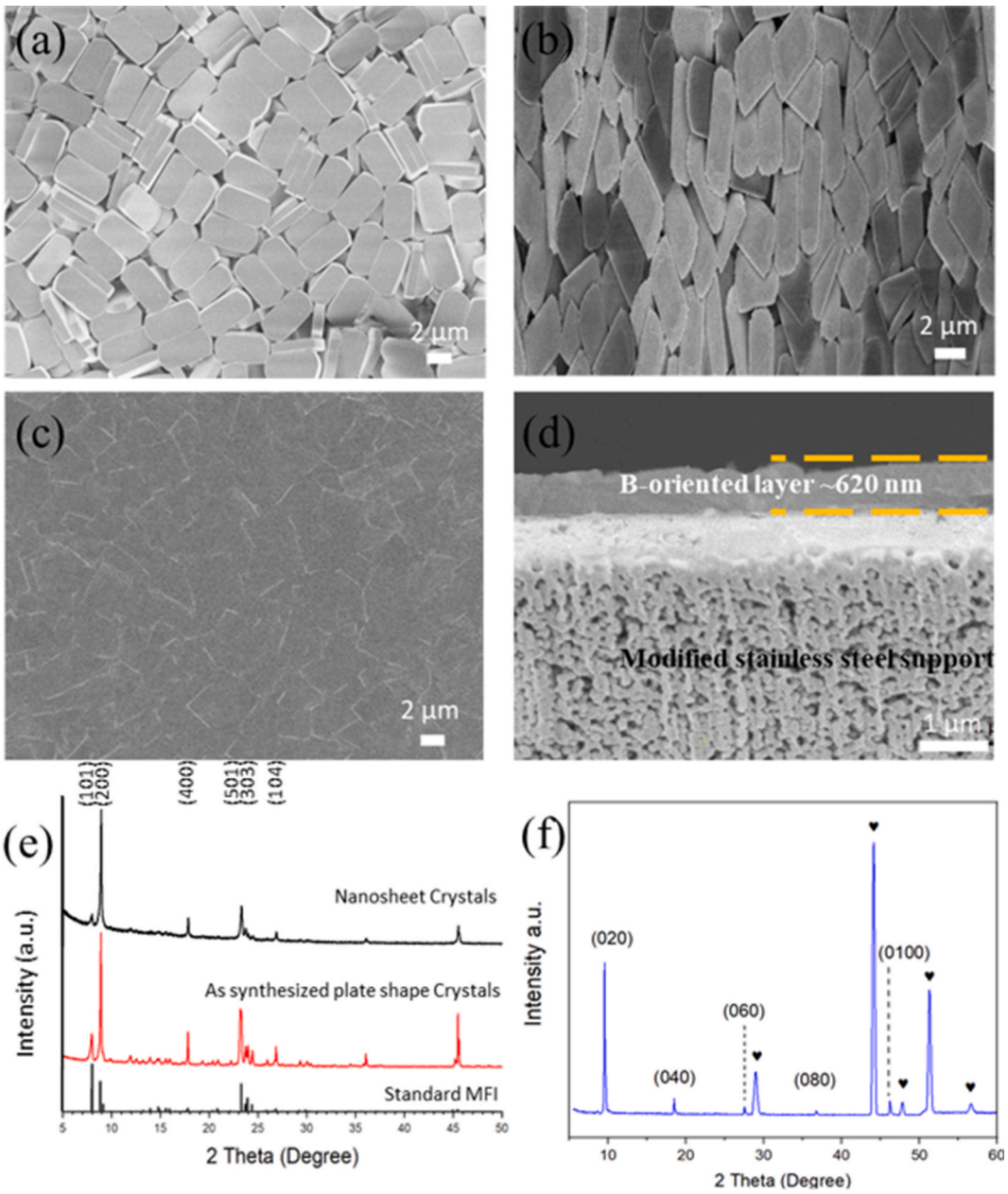

Fig. 8. SEM top-view of (a) the parent MFI crystals; (b) Nanosheet layer coated on substrate; (c) Membrane surface after secondary growth, (d) Cross section of membrane, XRD patterns of (e) parent MFI crystals, nanosheets and standard; (f) XRD pattern of b-oriented membrane, ♥ shows substrate peaks.

stainless-steel support after application of vacuum filtration (Fig. 8(b)). The XRD pattern of the as-synthesized parent plate-shaped crystals and the nanosheet crystals are presented in Fig. 8(e). XRD patterns further confirm the high purity and crystallinity of the obtained MFI nanosheet crystals. Moreover, for nanosheet crystals the XRD patterns show that the second hydrothermal step results in an enhancement in (020) plane (b-axis) peak intensity due to increase in the b/a and b/c aspect ratios.

Fig. 8(c) shows the SEM image of the membrane surface. The intergrown MFI nanosheets maintain their flat morphology, indicating that the primary growth of MFI and formation of newly nucleated crystals was suppressed during secondary growth step under optimized conditions. The cross-sectional image shows that the thickness of MFI layers are ~ 600 nm (Fig. 8(d)). X-ray diffraction (XRD) patterns further confirm the highly b-oriented MFI layer was obtained on modified stainless-steel substrate (Fig. 8(f)). The zeolite nanosheet coated support (Fig. 8(b)) and the synthesized b-oriented membrane (Fig. 8(c) and (d)) are shown in the last two steps in schematic diagram in Fig. 1.

The physical and chemical properties of supports are important to the synthesis of zeolite membranes and affect the performance of zeolite membranes on the supports. The support should have minimum gas transport resistance as compared to the coated zeolite layer. Table 1 compares permeance of several gases for the stainless-steel supports before and after modification conducted in this work, with a few supports reported in literature for growing b-oriented MFI zeolite membranes. Though alumina is the most common material used in the support for growing zeolite membranes [37], it was found difficult to grow b-oriented MFI zeolite membrane on alumina supports. Kumar et al. [18] reported supports made of Stöber silica, sintered silica fiber (SSF) supports made by pressing and sintering high-aspect-ratio silica fibers, and the SSF support coated with Stöber silica. Their supports have gas permeance in the order of 10^{-5}-10^{-6} mol/m^2 s Pa. The unmodified and modified stainless-steel supports studied in this work have similar gas permeance as those silica-based, mechanically weak supports reported in the literature. With permeance for stainless support starting at

Table 1
Single gas permeance data on a bare stainless-steel support, a stainless-steel support smoothened with the alloy, Si and SiO_2 particles, and a polished SSF support, an SSF support covered with the 500 nm Stöber silica particles, and a Stöber silica support.

Support	Permeance ($molm^{-2}s^{-1}Pa^{-1}$)		
	He	N_2	H_2
Stöber silica support [5,18]	3.7×10^{-6}	1.7×10^{-6}	5.6×10^{-6}
Polished SSF support [18]	3.9×10^{-5}	3.1×10^{-5}	7.5×10^{-5}
SSF support coated with 500 nm Stöber silica [18]	3.6×10^{-5}	2.9×10^{-5}	6.4×10^{-5}
SSF support coated with 500 nm and 50 nm Stöber silica [18]	3.5×10^{-5}	2.1×10^{-5}	5.5×10^{-5}
Bare stainless-steel support-This work	5.5×10^{-5}	2.8×10^{-5}	7.6×10^{-5}
Stainless-steel support coated Al–Si alloy-This work	5.1×10^{-5}	2.6×10^{-5}	7.3×10^{-5}
Stainless-steel support coated Al–Si ally and Si layers-This work	4.5×10^{-5}	2.2×10^{-5}	6.7×10^{-5}
Stainless-steel support Coated Al–Si alloy, Si and SiO_2 layers-This work	4.1×10^{-5}	1.9×10^{-5}	6.4×10^{-5}

Table 2
Xylene isomer separation results of MFI membranes measured for p-/o-xylene binary mixture feed.

Membrane	Temperature (°C)	P-x Permeance ($molm^{-2}\ s^{-1}\ Pa^{-1}$)	Separation Factor
Membrane A	150	1.52×10^{-7}	279
Membrane B	150	2.52×10^{-7}	388
Membrane C	120	9.7×10^{-8}	162

5×10^{-5} mol/m^2.s.Pa (for He), coating various layers only results in less than 20 % reduction in gas permeance, or increase in resistance. The gas permeance for the modified stainless supports is about 2 orders of magnitude larger than the permeance for the supported after coated with zeolites, indicating negligible resistance the support provides to the final zeolite membranes. The relative values of the gas permeance of He, N_2 and H_2 indicate a gas transport mechanism of combined Knudsen and viscous flow through these unmodified and modified stainless-steel supports, characteristic of gas transport through macropores.

The separation performance of the MFI membranes secondly-grown on the modified stainless supports with the MFI zeolite nanosheet seeds was evaluated for vapor permeation separation of p-/o-xylene equimolar binary mixture at a dilute feed at p-xylene and o-xylene partial pressures of ~0.49 kPa and ~0.55 kPa in He at total pressure of 1 atm. The kinetic diameters of the xylene isomers used are 0.58 nm for p-xylene and 0.68 nm for o-xylene. Table 2 lists xylene isomer separation performance for three b-oriented MFI zeolite membranes (A, B, and C) on the stainless-steel substrates modified by the same method. All these three membranes display high p-xylene permeance, good p-/o-xylene selectivity and stable performance. Membranes B and C were prepared at different secondary growth temperatures (150 °C and 120 °C, respectively). Since Membrane C exhibits a lower separation factor and permeance than Membrane B, this indicates that the reduced separation factor for Membrane C is unlikely due to the presence of more intercrystalline gaps compared to Membrane B. Instead, this difference is likely attributed to variations in the microstructure of MFI zeolite membranes resulting from the different growth temperatures.

Compared to random-oriented or c-oriented MFI zeolite membranes on alumina supports [38,39], the uniformly synthesized b-oriented zeolite membranes in this work have better xylenes separation performance due to integrated channel alignment, shorter diffusion lengths, fewer grain boundary defects, and ordered nanopore arrangement [8]. The b-oriented MFI zeolite membranes on the stainless-support synthesized this work exhibit lower p-/o-xylenes separation factor than some of the best b-oriented MFI zeolite membranes previously reported by the groups of Yoon [17] and Tsapatsis [1] (p-xylene permeance up to 3.2×10^{-7} mol m^{-2} $s^{-1}Pa^{-1}$ and p-/o-xylene separation factor of 480–8000) in 150–250 °C. However, their b-oriented MFI zeolite membranes were prepared on Stöber silica fiber supports with weak mechanical strength. It is a big challenge to scale up zeolite membranes on such supports [11,18]. B-oriented MFI zeolite membranes grown on macroporous alumina supports modified with microporous silica layer by sol-gel method [40,41] show xylene isomer separation factor and permeance in the same ranges as the values reported in Table 2. Numerous attempts were reported on synthesis of b-oriented MFI membranes on more scalable supports such as bare stainless-steel [42] and alumina [43], most of them lack xylene isomers separation performance data due to the difficult to grow high-quality b-oriented MFI zeolite membranes on these supports. The present study is the first to show success in synthesis of high-performance b-oriented MFI zeolite membranes on stainless-steel supports for xylene separation.

4. Conclusions

The study successfully synthesized high-selectivity, thin, b-oriented MFI zeolite membranes on modified stainless-steel supports. The surface modification of stainless-steel supports using Si–Al alloy, Si, and SiO_2 particles was effective, as evidenced by SEM images, XRD and FTIR analysis. Heat treatment of the Si–Al alloy layer is crucial for forming an outstanding adhesion layer on metal substrates, enhancing the interaction between the Si–Al alloy layer and stainless-steel support. Highly b-oriented 2D MFI nanosheet seeds derived from the plate-shape MFI zeolite crystals can be coated on the modified stainless support, leading to the synthesis of high p-/o-xylene selective b-oriented zeolite membranes. The successful synthesis is attributed to the integrated channel alignment and fewer grain boundary defects of the zeolite membrane on the modified supports. The reported advancements in productivity and scalability are critical to the industrial application of the b-oriented MFI zeolite molecular sieve membranes.

CRediT authorship contribution statement

Fateme Banihashemi: Writing – original draft, Methodology, Investigation, Formal analysis, Data curation. **Wen-Hsiung Lai:** Writing – review & editing, Formal analysis. **Jerry Y.S. Lin:** Writing – review & editing, Supervision, Resources, Project administration, Funding acquisition, Data curation, Conceptualization.

Declaration of competing interest

The authors declare the following financial interests/personal relationships which may be considered as potential competing interests: Jerry Y.S. Lin is Co-Editor-in-Chief Editor of the journal but was not involved in the peer review or handling of this paper.

Data availability

Data will be made available on request.

Acknowledgements

The authors gratefully acknowledge the financial support from National Science Foundation of the United States (CBET-2031087) and Department of Energy of the United States (DE0SC0024194).

References

[1] D. Kim, S. Ghosh, N. Akter, A. Kraetz, X. Duan, G. Gwak, N. Rangnekar, J. Johnson, K. Narasimharao, M.A. Malik, Twin-free, directly synthesized MFI nanosheets with improved thickness uniformity and their use in membrane fabrication, Sci. Adv. 8 (14) (2022) eabm8162.

[2] X. Wang, P. Karakiliç, X. Liu, M. Shan, A. Nijmeijer, L. Winnubst, J. Gascon, F. Kapteijn, One-pot synthesis of high-flux b-oriented MFI zeolite membranes for Xe recovery, ACS Appl. Mater. Interfaces 10 (39) (2018) 33574–33580, https://doi.org/10.1021/acsami.8b12613.

[3] L. Gora, J. Kuhn, T. Baimpos, V. Nikolakis, F. Kapteijn, E.M. Serwicka, Selective sensor utilizing a thin monolayer of b-oriented silicalite-1 crystals–magneto-elastic ribbon assembly, Analyst 134 (10) (2009) 2118–2122, https://doi.org/10.1039/B905039F.

[4] H. Xiao, J. Zhang, J. Dong, M. Luo, R. Lee, V. Romero, Synthesis of MFI zeolite films on optical fibers for detection of chemical vapors, Opt Lett. 30 (11) (2005) 1270–1272, https://doi.org/10.1364/OL.30.001270.

[5] T.C.T. Pham, H.S. Kim, K.B. Yoon, Growth of uniformly oriented silica MFI and BEA zeolite films on substrates, Science 334 (6062) (2011) 1533–1538, https://doi.org/10.1126/science.1212472.

[6] W.J. Roth, P. Nachtigall, R.E. Morris, J. Čejka, Two-dimensional zeolites: current status and perspectives, Chem. Rev. 114 (9) (2014) 4807–4837, https://doi.org/10.1021/cr400600f.

[7] U. Díaz, A. Corma, Layered zeolitic materials: an approach to designing versatile functional solids, Dalton Trans. 43 (27) (2014) 10292–10316, https://doi.org/10.1039/C3DT53181C.

[8] X. Lu, Y. Yang, J. Zhang, Y. Yan, Z. Wang, Solvent-free secondary growth of highly b-oriented MFI zeolite films from anhydrous synthetic powder, J. Am. Chem. Soc. 141 (7) (2019) 2916–2919, https://doi.org/10.1021/jacs.9b00018.

[9] H. Wang, Y.S. Lin, Effects of synthesis conditions on MFI zeolite membrane quality and catalytic cracking deposition modification results, Microporous Mesoporous Mater. 142 (2) (2011) 481–488, https://doi.org/10.1016/j.micromeso.2010.12.037.

[10] D. Kim, M.Y. Jeon, B.L. Stottrup, M. Tsapatsis, para-Xylene ultra-selective zeolite MFI membranes fabricated from nanosheet monolayers at the air–water interface, Angew. Chem. 130 (2) (2018) 489–494.

[11] B. Min, S. Yang, A. Korde, Y.H. Kwon, C. Jones, S. Nair, Continuous zeolite MFI membranes fabricated from 2D MFI nanosheets on ceramic hollow fibers, Angew. Chem. Int. Ed. 58 (2019), https://doi.org/10.1002/anie.201903554.

[12] M.Y. Jeon, D. Kim, P. Kumar, P.S. Lee, N. Rangnekar, P. Bai, M. Shete, B. Elyassi, H. S. Lee, K. Narasimharao, S.N. Basahel, S. Al-Thabaiti, W. Xu, H.J. Cho, E.O. Fetisov, R. Thyagarajan, R.F. DeJaco, W. Fan, K.A. Mkhoyan, J.I. Siepmann, M. Tsapatsis, Ultra-selective high-flux membranes from directly synthesized zeolite nanosheets, Nature 543 (7647) (2017) 690–694, https://doi.org/10.1038/nature21421.

[13] K. Varoon Agrawal, X. Zhang, B. Elyassi, D.D. Brewer, M. Gettel, S. Kumar, J. A. Lee, S. Maheshwari, A. Mittal, C.Y. Sung, M. Cococcioni, L.F. Francis, A. V. McCormick, K.A. Mkhoyan, M. Tsapatsis, Dispersible exfoliated zeolite nanosheets and their application as a selective membrane, Science (New York, N. Y.) 334 (6052) (2011) 72–75, https://doi.org/10.1126/science.1208891.

[14] K.V. Agrawal, B. Topuz, Z. Jiang, K. Nguenkam, B. Elyassi, L.F. Francis, M. Tsapatsis, M. Navarro, Solution-processable exfoliated zeolite nanosheets purified by density gradient centrifugation, AIChE J. 59 (9) (2013) 3458–3467, https://doi.org/10.1002/aic.14099.

[15] M. Zhou, J. Hedlund, Facile preparation of hydrophobic colloidal MFI and CHA crystals and oriented ultrathin films, Angew. Chem. 130 (34) (2018) 11132–11136.

[16] Y. Liu, W. Qiang, T. Ji, M. Zhang, M. Li, J. Lu, Y. Liu, Uniform hierarchical MFI nanosheets prepared via anisotropic etching for solution-based sub–100-nm-thick oriented MFI layer fabrication, Sci. Adv. 6 (7) (2020) eaay5993, https://doi.org/10.1126/sciadv.aay5993.

[17] T.C.T. Pham, T.H. Nguyen, K.B. Yoon, Gel-free secondary growth of uniformly oriented silica MFI zeolite films and application for xylene separation, Angew. Chem. Int. Ed. 52 (33) (2013).

[18] K.V. Agrawal, B. Topuz, T.C.T. Pham, T.H. Nguyen, N. Sauer, N. Rangnekar, H. Zhang, K. Narasimharao, S.N. Basahel, L.F. Francis, Oriented MFI membranes by gel-less secondary growth of sub-100 nm MFI-nanosheet seed layers, Adv. Mater. 27 (21) (2015) 3243–3249.

[19] Y. Gao, M. Chen, T. Zhang, X. Zheng, A novel method for the growth of ZSM-5 zeolite membrane on the surface of stainless steel, Mater. Lett. 65 (17) (2011) 2789–2792, https://doi.org/10.1016/j.matlet.2011.05.110.

[20] H.F. Chau, W.S. Tang, A cellular automaton model for the power law noise of an accretion disc, in: K.S. Cheng, H.F. Chau, K.L. Chan, K.C. Leung (Eds.), Stellar Astrophysics: Proceedings of the Pacific Rim Conference Held in Hong Kong, 1999, Springer, Netherlands, Dordrecht, 2000, pp. 257–266, https://doi.org/10.1007/978-94-010-0878-5_30.

[21] W. Stöber, A. Fink, E. Bohn, Controlled growth of monodisperse silica spheres in the micron size range, J. Colloid Interface Sci. 26 (1) (1968) 62–69, https://doi.org/10.1016/0021-9797(68)90272-5.

[22] B. Elyassi, M.Y. Jeon, M. Tsapatsis, K. Narasimharao, S.N. Basahel, S. Al-Thabaiti, Ethanol/water mixture pervaporation performance of b-oriented silicalite-1 membranes made by gel-free secondary growth, AIChE J. 62 (2) (2016) 556–563.

[23] v.E. Wicke, R. Kallenbach, Die oberflächendiffusion von kohlendioxyd in aktiven kohlen, Kolloid Z. 97 (2) (1941) 135–151.

[24] F. Banihashemi, J.Y.S. Lin, B-oriented MFI zeolite membranes for xylene isomer separation - effect of xylene activity on separation performance, J. Membr. Sci. 652 (2022) 120492, https://doi.org/10.1016/j.memsci.2022.120492.

[25] F. Banihashemi, L. Meng, A.A. Babaluo, Y.S. Lin, Xylene vapor permeation in MFI zeolite membranes made by templated and template-free secondary growth of randomly oriented seeds: effects of xylene activity and microstructure, Ind. Eng. Chem. Res. 57 (47) (2018) 16059–16068, https://doi.org/10.1021/acs.iecr.8b01373.

[26] V. Kumar, Effect of Chill Condition and Grain Refinement on the Microstructure and Mechanical Properties of B319 Aluminum Alloy, 2015.

[27] Z. Jiang, C. Li, S. Hao, K. Zhu, P. Zhang, An easy way for preparing high performance porous silicon powder by acid etching Al–Si alloy powder for lithium ion battery, Electrochim. Acta 115 (2014) 393–398, https://doi.org/10.1016/j.electacta.2013.08.123.

[28] S.-a. Tanusilp, N. Sadayori, K. Kurosaki, Nanostructured bulk Si for thermoelectrics synthesized by surface diffusion/sintering doping, RSC Adv. 9 (27) (2019) 15496–15501, https://doi.org/10.1039/C9RA02349F.

[29] P. Ma, Y. Jia, K.G. Prashanth, Z. Yu, C. Li, J. Zhao, S. Yang, L. Huang, Effect of Si content on the microstructure and properties of Al–Si alloys fabricated using hot extrusion, J. Mater. Res. 32 (11) (2017) 2210–2217, https://doi.org/10.1557/jmr.2017.97.

[30] C.R. Loayza, D.C.S. Cardoso, D.J.A. Borges, A.A.F. Castro, A.C. Bozzi, M.A.L. Dos Reis, E.M. Braga, Stainless steel-CNT composite manufactured via electric arc welding, Mater. Des. 223 (2022) 111169, https://doi.org/10.1016/j.matdes.2022.111169.

[31] M. Kopáni, M. Jergel, H. Kobayashi, M. Takahashi, R. Brunner, M. Mikula, K. Imamura, S. Jurečka, E. Pinčík, On determination of properties of ultrathin and very thin silicon oxide layers by FTIR and X - ray reflectivity, MRS Proceedings 1066 (2011), https://doi.org/10.1557/PROC-1066-A07-03.

[32] K.R. Lenhardt, H. Breitzke, G. Buntkowsky, E. Reimhult, M. Willinger, T. Rennert, Synthesis of short-range ordered aluminosilicates at ambient conditions, Sci. Rep. 11 (1) (2021) 4207, https://doi.org/10.1038/s41598-021-83643-w.

[33] T.F. Young, C.P. Chen, J.F. Liou, Y.L. Yang, T.C. Chang, Study on the Si–Si vibrational States of the near surface region of porous silicon, J. Porous Mater. 7 (2000) 339–343, https://doi.org/10.1023/A:1009622601723.

[34] G. Wardhani, N. Nurlela, M. Azizah, Silica content and structure from corncob ash with various acid treatment (HCl, HBr, and citric acid), Molekul 12 (2017) 174, https://doi.org/10.20884/1.jm.2017.12.2.382.

[35] M.E. Ayturk, E.E. Engwall, Y.H. Ma, Microstructure analysis of the intermetallic diffusion-induced alloy phases in composite Pd/Ag/porous stainless steel membranes, Ind. Eng. Chem. Res. 46 (12) (2007) 4295–4306, https://doi.org/10.1021/ie061677j.

[36] M.E. Ayturk, I.P. Mardilovich, E.E. Engwall, Y.H. Ma, Synthesis of composite Pd-porous stainless steel (PSS) membranes with a Pd/Ag intermetallic diffusion barrier, J. Membr. Sci. 285 (1) (2006) 385–394, https://doi.org/10.1016/j.memsci.2006.09.008.

[37] X. Lu, H. Wang, Y. Yang, Z. Wang, Microstructural manipulation of MFI-type zeolite films/membranes: current status and perspectives, J. Membr. Sci. 662 (2022) 120931, https://doi.org/10.1016/j.memsci.2022.120931.

[38] X. Gu, J. Dong, T.M. Nenoff, D.E. Ozokwelu, Separation of p-xylene from multicomponent vapor mixtures using tubular MFI zeolite mmbranes, J. Membr. Sci. 280 (1) (2006) 624–633, https://doi.org/10.1016/j.memsci.2006.02.020.

[39] J. O'Brien-Abraham, M. Kanezashi, Y.S. Lin, Effects of adsorption-induced microstructural changes on separation of xylene isomers through MFI-type zeolite membranes, J. Membr. Sci. 320 (1) (2008) 505–513, https://doi.org/10.1016/j.memsci.2008.04.023.

[40] Z. Lai, M. Tsapatsis, Gas and organic vapor permeation through b-oriented MFI membranes, Ind. Eng. Chem. Res. 43 (12) (2004) 3000–3007, https://doi.org/10.1021/ie034096s.

[41] Z. Lai, G. Bonilla, I. Diaz, J.G. Nery, K. Sujaoti, M.A. Amat, E. Kokkoli, O. Terasaki, R.W. Thompson, M. Tsapatsis, D.G. Vlachos, Microstructural optimization of a zeolite membrane for organic vapor separation, Science 300 (5618) (2003) 456–460, https://doi.org/10.1126/science.1082169.

[42] X. Li, Y. Yan, Z. Wang, Continuity control of b-oriented MFI zeolite films by microwave synthesis, Ind. Eng. Chem. Res. 49 (12) (2010) 5933–5938, https://doi.org/10.1021/ie1000136.

[43] X. Lu, Y. Peng, Z. Wang, Y. Yan, Rapid fabrication of highly b-oriented zeolite MFI thin films using ammonium salts as crystallization-mediating agents, Chem. Commun. 51 (55) (2015) 11076–11079, https://doi.org/10.1039/C5CC02980E.